New Journal of Physics
The open-access journal for physics

# Coulomb oscillations in three-layer graphene nanostructures

**J Güttinger**[1], **C Stampfer, F Molitor, D Graf, T Ihn and K Ensslin**
Solid State Physics Laboratory, ETH Zurich, 8093 Zurich, Switzerland
E-mail: guettinj@phys.ethz.ch

*New Journal of Physics* **10** (2008) 125029 (10pp)
Received 13 May 2008
Published 22 December 2008
Online at http://www.njp.org/
doi:10.1088/1367-2630/10/12/125029

**Abstract.** We present transport measurements on a tunable three-layer graphene single electron transistor (SET). The device consists of an etched three-layer graphene flake with two narrow constrictions separating the island from source and drain contacts. Three lateral graphene gates are used to electrostatically tune the device. An individual three-layer graphene constriction has been investigated separately showing a transport gap near the charge neutrality point. The graphene tunneling barriers show a strongly nonmonotonic coupling as a function of gate voltage indicating the presence of localized states in the constrictions. We show Coulomb oscillations and Coulomb diamond measurements proving the functionality of the graphene SET. A charging energy of $\approx$0.6 meV is extracted.

**Contents**

1. Introduction 2
2. Device and fabrication 2
3. Results and discussion 4
Acknowledgments 9
References 9

[1] Author to whom any correspondence should be addressed.

## 1. Introduction

Carbon materials, such as carbon nanotubes and graphene have attracted increasing interest in the past decades, which is mainly due to their unique electronic properties. High charge carrier mobilities in carbon nanotubes [1] and graphene [2, 3] make both materials interesting for future nanoelectronic applications [4, 5]. Their low atomic weight and the low nuclear spin concentration, arising from the ≈99% natural abundance of $^{12}C$ are good premises for having weak spin–orbit and hyperfine couplings. These make carbon nanomaterials also promising candidates for future spintronic devices [6, 7] and spin–qubit-based quantum computation [8]–[11]. It has been shown recently that nanotubes exhibit a topologically induced spin–orbit coupling [12], which is directly related to their cylindrical shape [13, 14]. In graphene and few-layer graphene such flux accumulating (circumferential) trajectories should not be present, leading to a legitimate hope for much weaker spin–orbit interaction and thus possible applications for spin-based quantum information processing. However, graphene and few-layer graphene quantum devices are still in their infancy since it is hard to confine carriers in these semi-metallic materials using electrostatic potentials.

Here, we report on Coulomb oscillations and Coulomb diamond measurements on an etched and fully tunable three-layer graphene single electron transistor (SET). SETs consist of a small island connected via tunneling barriers to source and drain contacts [15]. The first few-layer graphene SETs have been formed by Schottky barrier contacts on graphitic flakes [16] and just very recently etched single-layer graphene structures [17, 18] have been fabricated to demonstrate Coulomb blockade.

## 2. Device and fabrication

The investigated SET device is shown in figures 1(a)–(c) and consists of a three-layer graphene structure. Two ≈60 nm wide constrictions separate the graphene island from the source (S) and drain (D) contacts. The two constrictions are separated by about 1 $\mu$m, while the area of the island is $A \approx 0.1\,\mu m^2$. Two lateral side gates SG1 and SG2 allow to change the three-layer graphene barriers electrostatically and independently. The potential on the island can be separately changed by an additional side gate denoted as plunger gate (PG). The highly doped Si substrate is used as a back gate (BG) giving control over the overall Fermi level. Note that on the same flake an additional single constriction has also been fabricated (see inset in figure 2(a)).

The devices have been fabricated by mechanical exfoliation of graphite flakes on Si substrates covered with 295 nm thick $SiO_2$ as described in [19]. The individual graphite flakes were patterned by electron-beam (e-beam) lithography using 90 nm polymethyl methacrylate (PMMA) as resist and a subsequent reactive ion etching step by an $Ar/O_2$ plasma (9 : 1). Figure 1(b) shows a scanning force microscope (SFM) image of the etched three-layer graphene flake (bright area). A second e-beam lithography step followed by metallization and lift-off is used to place 2 nm Ti and 50 nm Au electrodes as shown in figure 1(c).

Confocal Raman spectroscopy measurements [20] have been used to determine the thickness of the graphitic flake, i.e. the number of graphene layers. A Raman spectrum recorded at the center of the three-layer graphene island is shown in figure 1(d). This spot is marked by a circle in the Raman image [21] of the device which is shown as an inset in figure 1(d). In this Raman image, white areas are attributed to the silicon oxide, bright (yellow) areas to the

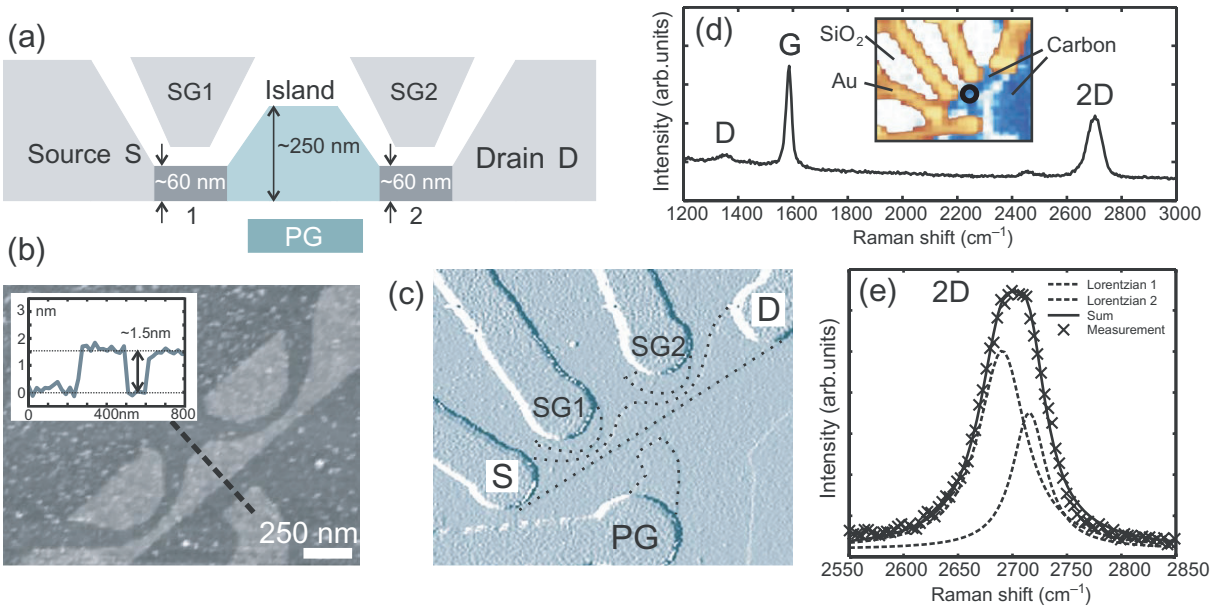


**Figure 1.** (a) Schematic illustration of the SET device. (b) SFM image of the device after reactive ion etching. The inset shows a cross section along the dashed line. (c) SFM image of the final device with metal contacts. The dotted lines indicate the circumference of the graphene structures. (d) Confocal Raman spectra recorded on the island after fabrication as highlighted in the Raman image shown as inset. The laser spot size is approx 400 nm. (e) The 2D line can be approximated by two Lorentzians. For more details see text.

contacts and dark (blue) areas to the three-layer graphene. Apart from the elevated background due to nearby metal contacts the spectrum shows pronounced G and 2D lines typical for $sp^2$ graphitic materials. The defect induced D line arises from the edges of the flake inside the area of the laser spot, which has a diameter of about 400 nm.

It is known from earlier experiments [20, 22, 23] that the intensity ratio of G/2D and the lineshape of the 2D peak provides direct insight into the number of graphene layers of the investigated flake. From the ratio between the integrated intensity of the G and the 2D line, which is $\approx 0.57$ for this flake, we can exclude bilayer graphene, since for two layers this ratio is $G/2D = 0.38 \pm 0.02$ [20]. For three (four, six) layers the integrated intensity ratio is $G/2D = 0.53 \pm 0.05$ ($G/2D = 0.63 \pm 0.08$, $G/2D = 0.7 \pm 0.1$) [20]. In addition, the 2D line is analyzed in more detail as shown in figure 1(e). According to [20], we can fit the 2D peak by the sum (straight line) of two Lorentzians (dashed lines in figure 1(e)) in order to analyze flakes consisting of more than two layers. The center of the two Lorentzians are offset by $\Delta\omega = 25.0 \pm 0.5\,\mathrm{cm}^{-1}$. It is found that our mesurements fit best to the value of three layers ($\Delta\omega = 25.4 \pm 1.5\,\mathrm{cm}^{-1}$) whereas for four (six) layers the two Lorentzians are expected to be offset by $\Delta\omega = 26 \pm 2\,\mathrm{cm}^{-1}$ ($\Delta\omega = 28 \pm 2\,\mathrm{cm}^{-1}$) [20]. This is also in good agreement with the step height of $\approx 1.5$ nm taken from the SFM data (inset and dashed line in figure 1(b)). However, four-layer graphene cannot be completely excluded here. In the following, we refer to our sample as consisting of three layers of graphene. The overall conclusions would not change if the sample had indeed four layers of graphene.

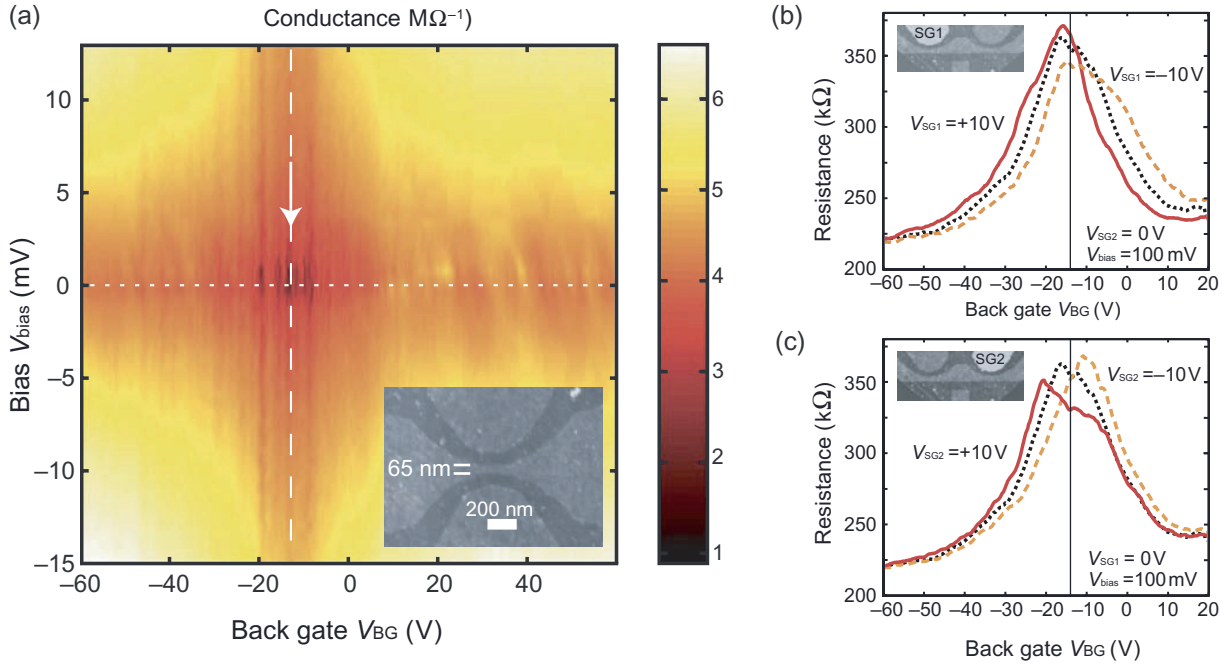


**Figure 2.** High bias source–drain current measurements. (a) Conductance as a function of bias and BG voltage for an individual three-layer graphene constriction (≈65 nm wide). A SFM image of the structure is shown in the inset. At low bias the opening of a transport gap is observed around $V_{BG} \approx -17$ V. (b) and (c) show BG characteristics for different side gate voltage configurations. In (b) $V_{SG2} = 0$ and the influence of SG1 is investigated for $V_{SG1} = 10$ V (line), 0 V (dotted) and −10 V (dashed line). In (c) $V_{SG1} = 0$ and the influence of SG2 is investigated for $V_{SG2} = 10$ V (line), 0 V (dotted) and −10 V (dashed line). A difference of the local doping of the two constrictions can be observed. For more information see text.

If not stated explicitly, measurements were performed at 2 K in a variable temperature cryostat by applying a symmetric source–drain bias voltage $V_{bias}$ (dc and small superimposed ac component) and measuring the source–drain current. The samples were heated up in vacuum to 135 °C for 12 h before cooling down to eliminate undesired atoms on the sample surface as much as possible.

## 3. Results and discussion

We first discuss measurements on a single constriction. This structure has been fabricated from the same graphene flake as the SET. The investigated constriction has a width of ≈65 nm, as shown in the inset of figure 2(a). Differential conductance measurements as functions of $V_{bias}$ and $V_{BG}$ (i.e. Fermi level) reveal the presence of a transport gap around the charge neutrality point (at $V_{BG} \approx -17$ V, see white arrow). This is indicated by (i) conductance suppressions near the charge neutrality point, including strong fluctuations for low bias, which might be due to resonances in the three-layer graphene constriction (see dark regions in figure 2(a)) and

(ii) the significant conductance nonlinearity as a function of increasing bias. This result is very similar to what has been measured in single-layer graphene nanoribbons [24, 25], where it has been argued that a nanoribbon-width-dependent effective energy gap (i.e. transport gap) dominates the transport near the charge neutrality point [26]. For the measured three-layer graphene constriction we observe the onset of a transport gap which is smaller than the thermal energy ($\approx k_B T = 0.2$ meV), since we do not observe any gap induced pinch off at small bias voltages. The gap is therefore significantly smaller than the $\approx$4 meV, which has been reported for 65 nm wide single-layer graphene constrictions [24, 26]. However, most importantly, three-layer graphene constrictions exhibit a transport gap which can be used to form tunneling barriers for defining a three-layer graphene island, very much like in single-layer graphene [17, 18].

Measurements on the SET are performed first in the high bias regime ($V_{bias} = 100$ mV), where transport is not suppressed by the two constrictions. This allows us to investigate different regimes in the back- and side gate parameter range. Figures 2(b) and (c) show the (two-point) source–drain resistance under the influence of different side gate potentials ($V_{SG1}$ is stepped in figure 2(b) and $V_{SG2}$ in figure 2(c)). The dotted traces show measurements where the side gate voltages have been set to zero. The dashed and the solid lines correspond to measurements where negative ($V_{SG1,2} = -10$ V) and positive ($V_{SG1,2} = 10$ V) side gate potentials have been applied, respectively. The resistance shows a peak around $V_{BG} = -15$ V, which we identify as the conductance minimum at the overall charge neutrality point of the significantly n-doped sample. For increasing or decreasing BG voltage the resistance decreases. This can be well explained by the (linear) carrier density increase as a function of the BG voltage when moving away from the charge neutrality point [19]. By applying different side gate potentials, the peak height width and position change. For example, setting $V_{SG1} = 10$ V and sweeping $V_{BG}$ the resistance peak becomes higher and narrower, while it is less pronounced and broader for $V_{SG1} = -10$ V (see figure 2(b)). The opposite behavior is observed for applying $\pm 10$ V to SG2, as shown in figure 2(c). In both cases a positive side gate voltage leads to a down shift in BG voltage, whereas a negative voltage leads to an upshift.

These transport characteristics can be well explained by assuming (i) that the transport in this regime is dominated by the two constrictions 1 and 2 and (ii) that the two constrictions are differently doped, i.e. they exhibit two different (local) charge neutrality points. Here constriction 2 is slightly more n-doped than constriction 1. According to [27] graphene side gates work well for locally changing the carrier density, i.e. for locally shifting the charge neutrality point. Moreover, we assume (as will be shown below) that the crosstalk of SG1 and SG2 on constrictions 2 and 1 is negligible. Therefore, a positive potential on SG1 reduces the doping imbalance between constrictions 1 and 2 (see figure 2(b)). This increases the sample homogeneity and results in a high and narrow resistance peak. In contrast, by applying $V_{SG1} = -10$ V the doping difference increases and the resistance peak significantly shrinks and broadens. The measurements shown in figure 2(c) can be explained similarly. Additionally, we can now extract the relative lever arms of the side gates to the BG with respect to the transport dominating constrictions given by $\Delta V_{SG1,2}/\Delta V_{BG} \approx 2.8$. From now on SG1 is operated in a positive and SG2 in a more negative voltage regime in order to match the doping levels in constrictions 1 and 2, which might lead to a more symmetric coupling of the island to source and drain.

We now discuss the low bias transport properties. Figure 3 shows a measurement of the source–drain current as a function of both side gates $V_{SG1}$ and $V_{SG2}$ performed at $V_{bias} = 200\,\mu$V and $V_{BG} = -13.47$ V. We observe sequences of horizontal and vertical stripes of suppressed

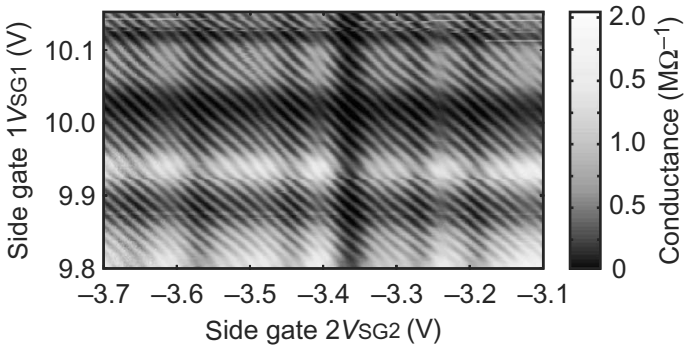


**Figure 3.** Source–drain current plotted as function of the two side gates voltages $V_{SG1}$ and $V_{SG2}$ for constant bias voltage ($V_{bias} = 200\,\mu V$). Measurements are taken at $V_{BG} = -13.47\,V$ and $V_{PG} = 0\,V$.

current and current resonances. Their direction in the $V_{SG1}$–$V_{SG2}$-plane indicates that their physical origin has to be found within constriction 1 (vertical stripes) or constriction 2 (horizontal stripes). The current exhibits even finer equidistantly spaced resonances which are almost equally well tuned by both side gates. We therefore attribute these resonances to states localized on the island between the barriers. It will be shown below that these resonances are Coulomb oscillations due to charging of the three-layer graphene island. The overall behavior is very similar to what has been observed in a single layer graphene SET [17].

Coulomb oscillations are further investigated by modulating the PG voltage $V_{PG}$ and simultaneously compensating its influence on the constrictions by the side gates respectively. Figure 4 shows the current as a function of $V_{PG}$. Here, SG1 has been swept simultaneously following $V_{SG1} = 6\,V - 0.27 V_{PG}$. The PG induced background modulation due to resonances in constriction 2 is negligible within this $V_{PG}$ range and has therefore not been compensated. For these measurements $V_{bias} = 50\,\mu V$ has been applied and the BG voltage has been set to $V_{BG} = -10.51\,V$. Thus the Fermi energy in the source and drain contacts lies within the conduction band. In accordance with the measurement in figure 3, the current shows coarse and fine modulations. Again the larger oscillations with characteristic $V_{PG}$ spacings of a few volts (see e.g. figure 4(a)) are attributed to transmission resonances in the constrictions while the fine current modulations at a voltage scale of around 30 mV are Coulomb oscillations, as shown in figure 4(b). The elevated background at the left side in figure 4(b) is due to resonances in the constrictions. The inset in figure 4(a) shows the spacing of the Coulomb oscillations $\Delta V_{pp}$ as function of the PG voltage, which has been swept over more than 150 periods. The gray marked region corresponds to the oscillations shown in figure 4(b). The mean Coulomb peak spacing is $\Delta V_{pp} = 30.1 \pm 2\,mV$ and part of the observed broadening might be due to the underlying modulation of the transmission through the narrow constriction (see correlation between figure 4(a) and inset in figure 4(b)). The essentially constant peak spacing indicates that the three-layer graphene transistor compared to the single layer graphene SET [17] behaves much more like a metallic SET [28]. One also needs to take into account that the three-layer device investigated here is larger than the single layer device presented in [17]. Therefore, the single-level spacing which could give rise to peak spacing fluctuations is also smaller. Nevertheless the data in the inset of figure 4(b) resembles pretty much observations on metallic SET with the additional feature of superposed constriction resonances. Like for the single-layer

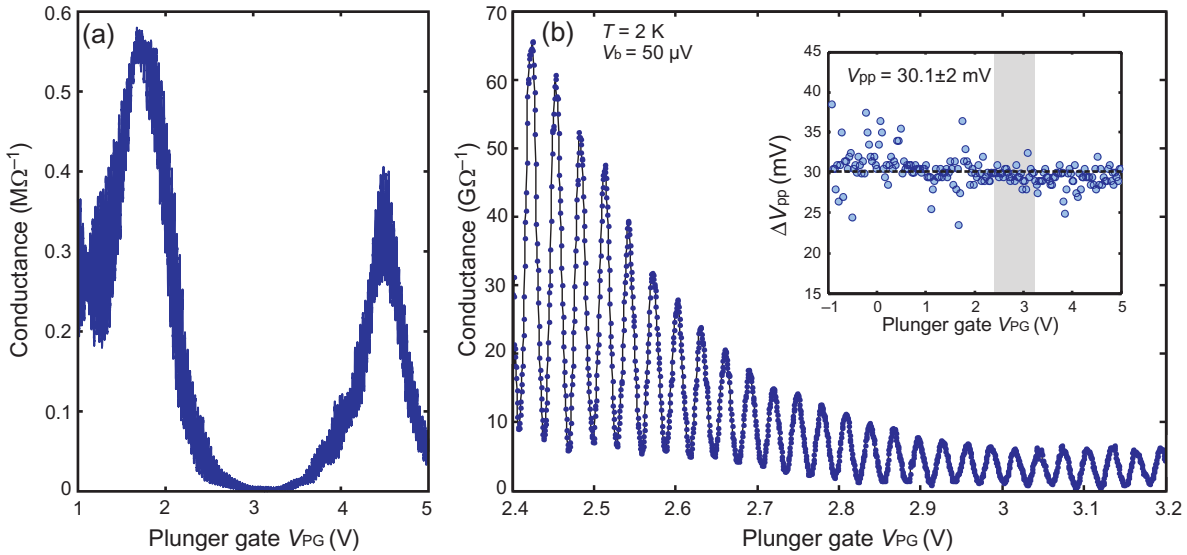


**Figure 4.** Coulomb oscillations (figure (b)) as a function of the PG voltage $V_{PG}$. Although the background is strongly modulated by constriction resonances (see figure (a)) an almost constant peak spacing is observed over more than 150 oscillations (see inset in figure (b)). Measurements are taken at $V_{SG1} = 6\,\mathrm{V} - 0.27 V_{PG}$, $V_{SG2} = -2.37\,\mathrm{V}$, $V_{BG} = -10.51\,\mathrm{V}$ and $V_{bias} = 50\,\mu\mathrm{V}$.

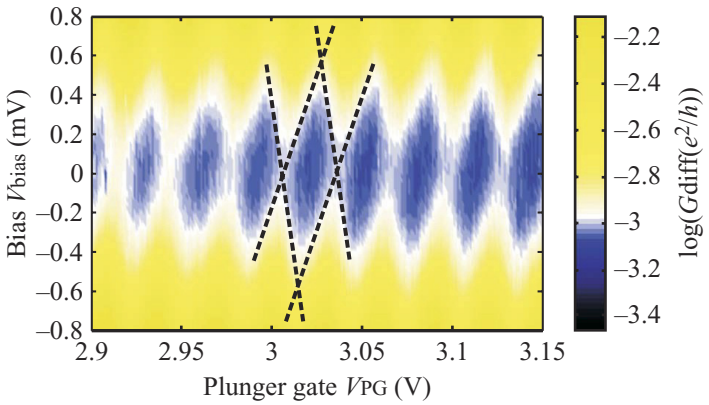


**Figure 5.** Coulomb diamond measurements. From the size of the Coulomb diamonds we estimate a value for the charging energy of around 0.6 meV. The dc bias is modulated with a 50 $\mu$V ac component allowing for a direct lock-in amplifier measurement of the differential conductance. The measurement is performed with $V_{SG1} = 6\,\mathrm{V} - 0.27 \cdot V_{PG}$, $V_{SG2} = -2.37\,\mathrm{V}$ and $V_{BG} = -10.51\,\mathrm{V}$.

graphene SET, some peak spacing fluctuations can be seen in figure 3 indicating that weak inhomogeneities exist within the dot including its edges.

Corresponding Coulomb diamond measurements [15], i.e. measurements of the differential conductance ($G_{diff} = \mathrm{d}I/\mathrm{d}V_{bias}$) as a function of bias voltage $V_{bias}$ and PG voltage $V_{PG}$ are shown in figure 5. For this measurement the same gate voltage configuration as in figure 4 has been used and an ac modulation of 50 $\mu$V has been superimposed on to the dc bias. The

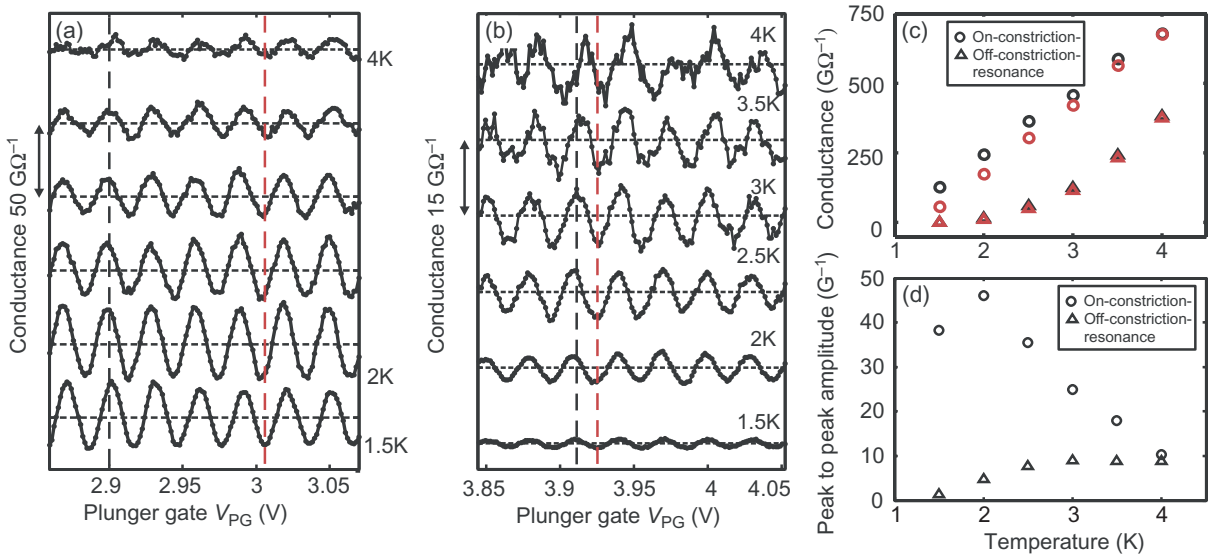


**Figure 6.** Temperature dependence of Coulomb oscillations (COs) in two different regimes. (a) COs sitting on top of a constriction resonance ('on-constriction-resonance'). (b) COs in a regime where the current is strongly suppressed by the constrictions ('off-constriction-resonance'). (c) Current measured at the PG voltages indicated by the dashed lines in (a) and (b) for both regimes. (d) Temperature dependence of the COs peak to peak amplitude. Measurements taken at $V_{SG1} = 5.067\,\mathrm{V} - 0.27(V_{PG} - 3.437\,\mathrm{V})$, $V_{SG2} = -1.588\,\mathrm{V}$, $V_{BG} = -10.51\,\mathrm{V}$ and $V_{bias} = 200\,\mu\mathrm{V}$.

differential conductance is plotted logarithmically as function of the PG and bias voltage. From this measurement the charging energy is estimated to be $E_C \approx 0.6\,\mathrm{meV}$. This corresponds to a total capacitance of $C_\Sigma = e^2/E_C \approx 271\,\mathrm{aF}$. The electrostatic coupling capacitances of the different gates to the island are $C_{PG} \approx 7.1\,\mathrm{aF}$, $C_{SG1} \approx 8.5\,\mathrm{aF}$, $C_{SG2} \approx 7.1\,\mathrm{aF}$ and $C_{BG} \approx 28.45\,\mathrm{aF}$. The capacitance of the island to the BG $C_{BG}$ can be compared with a parallel plate capacitor model leading to a capacitance $C = \epsilon_0 \epsilon A/d \approx 12\,\mathrm{aF}$. The difference to the capacitance obtained from the measurement can be explained by additional fields at the edges which are not accounted for in the simple plate capacitor model. These measurements are in accordance to what has been observed for a single-layer graphene SET [17]. There the island area is significantly smaller, leading to a larger charging energy ($\approx 3.5\,\mathrm{meV}$) and a larger discrepancy between the BG capacitance and the plate capacitor model is observed due to the even more enhanced edge effects of the smaller island.

Finally, we investigate the temperature dependence of the Coulomb oscillations and the background (i.e. constriction) resonances in two different PG regimes. Within the first regime the background is strongly elevated, whereas in the second regime the background is strongly suppressed since we are between two constriction resonances. The Coulomb oscillations on top of a constriction resonance are plotted for different temperatures in figure 6(a). Here the background has been subtracted and the traces are vertically offset by 10 pA for clarity. In figure 6(b), the data are presented in the same way for the off-resonance regime in the barrier transmission with a spacing of 3 pA between the traces. The change of the background

current is shown in figure 6(c), where the current is plotted for two fixed PG voltages indicated by the vertical dashed lines in figures 6(a) and (b). On top of the constriction resonance (circles) the background current increases linearly with temperature, which does not hold for the regime with suppressed transmission ('off-constriction-resonance', triangles). There, the nonlinear current increase is attributed to raising and subsequent broadening of constriction resonances lifting the overall background current. Figure 6(d) shows the averaged peak to peak Coulomb oscillation amplitudes. While the 'on-constriction-resonance' amplitudes (circles) of the Coulomb oscillations are in general decreasing with increasing temperature, the amplitudes off the 'off-constriction-resonance' oscillations (triangles) are mainly limited by the transmission of the constrictions and therefore increase due to enhanced transmission (elevated background) with increasing temperature.

In conclusion, we have fabricated a tunable three-layer graphene SET based on an etched graphitic flake with lateral gates. Its functionality was demonstrated by observing clear and reproducible Coulomb oscillations. The tunneling barriers formed by three-layer graphene constrictions were investigated independently. From the Coulomb diamond measurements it was estimated that the charging energy of the three-layer graphene island is $\approx 0.6$ meV, which is compatible with its lithographic dimensions. The overall behavior of the investigated device is very much like that observed for a single-layer graphene SET. The almost constant Coulomb peak spacing indicates the more metallic character of the three layer graphene SET. These results open the way to more detailed studies of future graphene and few-layer graphene quantum devices.

## Acknowledgments

We thank R Leturcq, P Studerus, C Barengo and K Novoselov for helpful discussions. Support by the ETH FIRST Lab and financial support by the Swiss National Science Foundation and NCCR nanoscience are also gratefully acknowledged.

## References

[1] Ando T, Nakanishi T and Saito R 1998 *J. Phys. Soc. Japan* **67** 2857
[2] Novoselov K S, Geim A K, Morozov S V, Jiang D, Katsnelson M I, Grigorieva I V, Dubonos S V and Firsov A A 2005 *Nature* **438** 197–200
[3] Zhang Y, Tan Y W, Stormer H L and Kim P 2005 *Nature* **438** 201–4
[4] Geim A K and Novoselov K S 2007 *Nat. Mater.* **6** 183
[5] Avouris P, Chen Z H and Perebeinos V 2007 *Nat. Nanotechnol.* **2** 605
[6] Awschalom D D and Flatt M E 2007 *Nat. Phys.* **3** 153
[7] Tombros N, Jozsa C, Popinciuc M, Jonkman H T and van Wees B J 2007 *Nature* **448** 571
[8] Loss D and DiVincenzo D P 1998 *Phys. Rev.* A **57** 120
[9] Elzerman J M, Hanson R, Willems van Beveren L H, Witkamp B, Vandersypen L M K and Kouwenhoven L P 2004 *Nature* **430** 431–5
[10] Petta J R, Johnson A C, Taylor J M, Laird E A, Yacoby A, Lukin M D, Marcus C M, Hanson M P and Gossard A C 2005 *Science* **309** 2180–84
[11] Trauzettel B, Bulaev D V, Loss D and Burkard G 2007 *Nat. Phys.* **3** 192
[12] Kuemmeth F, Ilani S, Ralph D C and McEuen P L 2008 *Nature* **452** 448
[13] Ando T 2000 *J. Phys. Soc. Japan* **69** 1757–63
[14] Huertas-Hernando D, Guinea F and Brataas A 2006 *Phys. Rev.* B **74** 155426

[15] Kouwenhoven L P *et al* 1997 *Electron Transport in Quantum Dots* (*Mesoscopic Electron Transport*) ed L L Sohn, L P Kouwenhoven and G Schön (Dordrecht: NATO Series, Kluwer)
[16] Bunch J S, Yaish Y, Brink M, Bolotin K and McEuen P L 2005 *Nano Lett.* **5** 287–90
[17] Stampfer C, Güttinger J, Molitor F, Graf D, Ihn T and Ensslin K 2008 *Appl. Phys. Lett.* **92** 012102
[18] Ponomarenko L A, Schedin F, Katsnelson M I, Yang R, Hill E H, Novoselov K S and Geim A K 2008 *Science* **320** 320–58
[19] Novoselov K S, Geim A K, Morozov S V, Jiang D, Katsnelson M I, Dubonos S V, Grigorieva I V and Firsov A A 2004 *Science* **306** 666
[20] Graf D, Molitor F, Ensslin K, Stampfer C, Jungen A, Hierold C and Wirtz L 2007 *Nano Lett.* **7** 238
[21] Stampfer C, Bürli A, Jungen A and Hierold C 2007 *Phys. Status Solidi* b **244** 4341–45
[22] Ferrari A C *etal* 2006 *Phys. Rev. Lett.* **97** 187401
[23] Gupta A, Chen G, Joshi P, Tadigadapa S and Eklund P C 2006 *Nano Lett.* **6** 2667
[24] Han M Y, Özyilmaz B, Zhang Y and Kim P 2007 *Phys. Rev. Lett.* **98** 206805
[25] Chen Z, Lin Y M, Rooks M J and Avouris P 2007 *Physica* E **40** 228–32
[26] Sols F, Guinea F and Castro Neto A H 2007 *Phys. Rev. Lett.* **99** 166803
[27] Molitor F, Güttinger J, Stampfer C, Graf D, Ihn T and Ensslin K 2007 *Phys. Rev.* B **76** 245426
[28] Furlan M, Heinzel T, Jeanneret B, Lotkhov S V and Ensslin K 2000 *Europhys. Lett.* **49** 369